STABILITY AND WIDTH OF REACTION FRONTS IN 3D POROUS MEDIA

Magnus Wangen[1,*]

[1]*Institute for Energy Technology, P.O.Box 40, N-2027 Kjeller, Norway*

[*]Address all correspondence to Magnus Wangen E-mail: Magnus.Wangen@ife.no

Original Manuscript Submitted: 25/11-2011; Final Draft Received:

Transport of reactive fluids in porous media may form reaction fronts – narrow zones where the reaction takes place. We derive approximate solutions for the change in concentration and porosity across the front zone. These solutions are used to derive a condition for reaction fronts to be narrow. Reaction fronts tend to be unstable and they often show a fingered growth into the porous medium. A criterion for the stability of sharp reaction fronts in a 3D homogeneous porous medium is derived using linear stability analysis. The criterion gives that a perturbation of a flat reaction front of any wave-length becomes unstable if the permeability behind the front increases. The front instability grows faster for short wave lengths than for long wave lengths. Similarly, the perturbations of the front will die out if the permeability behind the front decreases, and short wave length perturbations will die out faster than long wave length perturbations. Front stability and the stability criterion are demonstrated with numerical examples where the fronts are narrow, but not sharp.

KEY WORDS: *Reaction fronts in porous media, front stability, numerical simulation*

1. INTRODUCTION

The injection of a reactive fluid in a porous medium may lead to reaction fronts – zones where the medium goes from unreacted to fully reacted. Reaction fronts may propagate in a finger like way into the porous medium, in which case the front propagation is an unstable process. Reaction fronts play an important part in a number of geochemical processes such as contamination of groundwater (Cherry et al., 1984), diagenesis (Dewers and Ortoleva, 1994), melt migration (Daines and Kohlstedt, 1994) and cave formation (Szymczak and Ladd, 2011). Laboratory examples of sharp reaction fronts are dissolution of calcite minerals in sandstone cores using acid, where a quartzose matrix is left behind as the carbonates are dissolved (Rege and Fogler, 1989).

It is often of interest to know when the reaction fronts are narrow. Lichtner (1988); Steefel and Lasaga (1990); Szymczak and Ladd (2009); Zhao et al. (2008) have derived solutions of the concentration equation that give insight into the spatial extent of the reaction. Here we derive a condition for when a reaction zone becomes narrow. Furthermore, we extend the concentration solution across the front to an approximate solution for the porosity.

Dissolution reactions lead to an increased porosity and thereby an increased permeability. The coupling of reaction and flow, by means of the porosity and permeability, may lead to reaction fronts that propagate into the porous medium as an unstable process. This instability was first studied by Chadam et al. (1987, 1988), Ortoleva et al. (1987), Sherwood (1987) and Hinch and Bhatt (1990). These authors analyze the stability of a reaction front in 2D using a linear stability analysis and different assumptions regarding the front. Chadam et al. (1987, 1988) and Ortoleva et al. (1987) derived a stability condition assuming a sharp front in porosity and permeability, but not in the concentration. Sherwood (1987) and Hinch and Bhatt (1990) have a different approach where

they assume a constant porosity, but have the permeability dependent on the amount of dissoluble minerals. They ignore diffusion and obtain analytic results for small and large wave-numbers and for small variations in the permeability.

These earlier stability analyzes are all in 2D. Here we derive an analytic stability criterion for sharp reaction fronts in a 3D homogeneous porous medium, assuming that the front is sharp in porosity, permeability and concentration. The sharp front assumption gives a stability condition that applies in 3D for any wave-length of the front perturbation and for any permeability contrast across the front. The stability analysis is based on the same technique as the gravitational instability of an interface between two immiscible fluids in a vertical Hele-Shaw cell (Saffman and Taylor, 1958), and the chosen approach follows the linear stability analysis presented by Marle (1981).

The stability criterion is demonstrated with a numerical model based on a one-component reaction-convection-diffusion equation coupled to Darcy flow and dissolution. The dissolution changes the porosity and therefore the permeability. These experiments indicate that the stability criterion may by useful in the interpretation of a wide variety of reaction fronts in geology and engineering.

This paper is organized as follows: The continuum equations for reaction-transport are presented. The assumptions about specific surface and permeability as a function of porosity are discussed. The condition for a narrow front is given, before the stability criterion of reaction fronts in porous media is presented.

2. REACTION AND TRANSPORT MODELLING

The numerical reaction fronts are modelled with 3 coupled equations in an isothermal porous medium (Chadam et al., 1988; Ortoleva et al., 1987; Xin et al., 1993). The domain is a rectangular box where the inlet is at one side and the outlet is at the opposite side. Conservation of fluid mass combined with Darcy's law give the pressure equation (Chadam et al., 1988; Ortoleva et al., 1987; Xin et al., 1993)

$$\nabla \cdot \Big(\frac{k}{\mu} \nabla p_e \Big) = \frac{\partial \phi}{\partial t} \tag{1}$$

The Darcy flux $\mathbf{u}_D = -(k/\mu)\nabla p_e$ is proportional to the gradient of the overpressure p_e, where the overpressure is the fluid pressure minus the hydrostatic fluid pressure. The permeability field $k(\mathbf{x}, \phi)$ is a scalar function of both position and porosity, where the dependence on porosity becomes important when dissolution takes place. The viscosity is denoted by μ. The fluid density and the rock density are taken to be constant. Boundary conditions for the pressure equation is a constant flow rate at the inlet (at the left) and zero pressure at the outlet (to the right).

A solution of the pressure equation gives the Darcy flux, which together with diffusion, drive the transport of the solute. The flux of dissolved matter due to fluid flow and diffusion in the pore fluid is

$$\mathbf{F} = c\,\mathbf{u}_D - \phi D \nabla c, \tag{2}$$

where the concentration of solute is denoted c (mole m^{-3}) and the diffusivity is D ($\mathrm{m}^2\mathrm{s}^{-1}$). A mass balance in terms of the number of moles of solute in a fixed volume gives the equation

$$\frac{\partial(\phi c)}{\partial t} + \nabla \cdot \Big(c\,\mathbf{u}_D - \phi D \nabla c \Big) = k_d\, S(\phi) \left(1 - \frac{c}{c_{\mathrm{eq}}} \right), \tag{3}$$

where the right-hand-side is the source term that represents dissolution by first order kinetics (Chadam et al., 1988; Lichtner, 1996; Ortoleva et al., 1987; Xin et al., 1993). The coefficient k_d is the dissolution rate (mole $\mathrm{s}^{-1}\mathrm{m}^{-2}$), c_{eq} is the equilibrium concentration of dissolved species in the pore fluid and S is the reactive specific surface area (m^{-1}). The specific surface area is dependent on the dissolution process through the porosity.

The rate of change of porosity is written as

$$\frac{\partial \phi}{\partial t} = -\mathcal{V}_s c_{\mathrm{eq}}\, K_d\, \hat{S}\Big(\frac{\phi}{\phi_1} \Big)\, C \;\text{ when }\; C < 0, \tag{4}$$

where $\mathcal{V}_s$ is the molar volume of the solid and where we have introduced the degree of supersaturation

$$C = \frac{c}{c_{\mathrm{eq}}} - 1, \tag{5}$$

Brine with zero solute has then $C = -1$ and brine in equilibrium with the solid has $C = 0$. The specific surface area is written as

$$S(\phi) = S_0 \cdot \hat{S}\Big(\frac{\phi}{\phi_1} \Big), \tag{6}$$

where S_0 is the initial specific surface area at the initial porosity ϕ_1. The function $\hat{S}$ takes care of how the specific

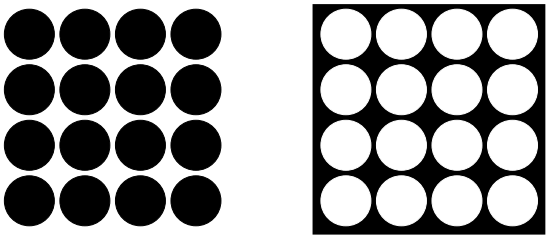

(a) (b)

FIG. 1: Black is solid and white is void space. (a) Pore space between grains. (b) Pore space as holes in well cemented rock.

surface area develops with changing porosity, and it gives the value 1 for $\phi = \phi_1$. The initial specific surface area is used to form the dissolution coefficient

$$K_d = \frac{k_d\, S_0}{c_{\rm eq}}, \tag{7}$$

with units s^{-1}. The reaction and transport equation (3) can also be written as

$$\phi \frac{\partial C}{\partial t} + \mathbf{u}_D \cdot \nabla C - \nabla \cdot \Big(\phi\, D \nabla C\Big) = -K_d\, \hat{S}\Big(\frac{\phi}{\phi_1}\Big)\, C, \tag{8}$$

using the pressure equation (1).

The three equations (1), (3) and (4) are the basis for the numerical reaction-transport modelling. These three equations are solved sequentially at each time step. The pressure equation is solved first with an implicit finite difference scheme. The pressure gives the Darcy flux, which is inserted into the reaction-transport equation. This equation is solved by an implicit finite difference scheme, where also the source term is handled implicitly. The concentration from the reaction-transport equation is then used to update the porosity, which is done with a fourth-order Runge-Kutta scheme.

The boundary conditions for the concentration equation are zero concentration ($C = -1$) at the left side (the fluid entrance) and the equilibrium concentration ($C = 0$) at the right side (the fluid exit). The other sides are closed for fluid flow. The pore fluid is initially in equilibrium with the solid ($C = 0$).

3. SPECIFIC SURFACE AND POROSITY EVOLUTION

The specific reactive surface as a function of the porosity is a difficult property to predict. Ortoleva et al. (1987) derives a function of the form

$$S(\phi) = S_0 \cdot \Big(\frac{\phi_2 - \phi}{\phi_2 - \phi_1}\Big)^{2/3}, \tag{9}$$

for the specific surface area of a packing of grains, where ϕ_2 is the finial porosity that remains when all dissolvable parts have gone into solution. A more elaborate version of this model is the fully penetrable sphere model (Elsner et al., 2009; Torquato, 1991; Weissberg, 1963). With the fully penetrable sphere model it is possible to consider an inverse porous medium where solid and void are interchanged. Here, we approximate the specific surface function as follows for a cemented rock with an inverse model

$$S(\phi) = S_0 \cdot \Big(\frac{\phi}{\phi_1}\Big)^{m} \tag{10}$$

by using an exponent $m = 1$. A difference between the two alternatives (9) and (10) is that the specific surface area for grains decreases with increasing porosity, while the function (10) for cemented rocks gives an increasing specific surface area with increasing porosity. This effect is illustrated with figure 1, where the surface area in figure 1a decreases with decreasing grains, while it increases in figure 1b with increasing pores. Therefore, the inverse model could be a better choice for a well cemented rock than the grain model. The relationship (10) is a simple mean to approximate the specific surface area of a number of different cemented rocks.

Changes in the porosity lead to changes in the permeability. The permeability is assumed to follow a Kozeny-Carman-like function of the porosity

$$k(\phi) = k_0 \left(\frac{\phi}{\phi_1}\right)^{n}, \tag{11}$$

where the exponent is $n = 3$.

4. THE TIME SCALES OF THE MODEL

The behaviour of the concentration equation can be described in terms of two dimensionless numbers – the Péclet- and the Damköhler-numbers. These numbers appear as the only two parameters in a scaled 1D version

of the reaction-transport equation (3), when it is made dimensionless by scaling x-coordinate, porosity and time as $\hat{x} = x/l_0$, $\hat{\phi} = \phi/\phi_1$ and $\hat{t} = t/t_0$, respectively, where l_0 is the length of the box and

$$t_0 = \frac{l_0^2}{D}, \tag{12}$$

is the time characteristic for diffusion over a distance l_0. The following dimensionless 1D equation is then obtained

$$\hat{\phi}\frac{\partial C}{\partial \hat{t}} + \mathrm{Pe}\,\frac{\partial C}{\partial \hat{x}} - \frac{\partial}{\partial \hat{x}}\Big(\hat{\phi}\,\frac{\partial C}{\partial \hat{x}}\Big) = -\mathrm{Da}\,C, \tag{13}$$

where the two parameters

$$\mathrm{Pe} = \frac{l_0 u_{D0}}{\phi_1 D} \quad \text{and} \quad \mathrm{Da} = \frac{l_0^2\,K_d}{\phi_1 D}, \tag{14}$$

are the Péclet-number and the Damköhler-number, respectively. The right-hand-side is simplified by letting $\hat{S}(\phi) = 1$. Both the Pe- and the Da-number include the initial porosity, and equation (13) applies for a simplified system where the porosity increase is negligible. Scaling the porosity makes the Pe- and the Da-numbers the only parameters in the model as long as the porosity does not change much. The Pe- and the Da-numbers can be expressed by the three time scales inherent in the reaction-transport equation (3). The first is t_0, the second is the time needed to flood the sample with one pore volume

$$t_p = \frac{\phi_1 l_0}{u_{D0}}, \tag{15}$$

and the third is the characteristic time of the dissolution process

$$t_d = \frac{\phi_1}{K_d}. \tag{16}$$

These three time scales give the Pe- and the Da-numbers as follows

$$\mathrm{Pe} = \frac{t_0}{t_p} \quad \text{and} \quad \mathrm{Da} = \frac{t_0}{t_d}. \tag{17}$$

The Pe-number measures the time scale of diffusion relative to the time scale of advection. The Da-number measures the time scale of diffusion relative to the time scale of dissolution. The dimensionless 1D equation (13) allows for simple solutions in case of constant porosity, which can be useful both for testing and interpretation of the reaction-transport model.

5. CONDITION FOR A NARROW REACTION FRONT

A reaction front is a narrow zone where the porous medium goes from completely unreacted to fully reacted. The concentration and porosity resulting from a reaction-transport process do not necessarily give a front. A condition for a narrow front-zone is therefore wanted. Such a condition can be obtained by considering a 1D stationary solution relative to the front. We introduce the x-coordinate $x' = x - v_f t$ as the distance from the front, where v_f is the front velocity. If the concentration has the same shape relative to the front we then have a stationary solution of the form

$$C(x') = C(x - v_f t). \tag{18}$$

When equation (18) is inserted into the 1D version of the concentration equation (8) we obtain the stationary equation

$$u'_D\frac{dC}{dx'} - \frac{d}{dx'}\Big(\phi\,D\frac{dC}{dx'}\Big) = -K_d\,C \tag{19}$$

after making the replacement $d/dx = d/dx'$. The condition for a narrow front is derived for small changes in the porosity and the specific surface is therefore approximated as $\hat{S}(\phi) \approx 1$. We notice that $u'_D = u_D - \phi v_f$ is the Darcy flux in the x'-coordinate system that follows the front. In order to allow for a solution of the concentration equation (19) it is first assumed that the porosity makes a jump at the front, which gives that $\phi = \phi_2$ for $x' < 0$ (behind the front) and $\phi = \phi_1$ for $x' \geq 0$ (ahead of the front). The concentration equation (19) is solved with boundary conditions

$$C(x' \to -\infty) = C_{\mathrm{in}} \quad \text{and} \quad C(x' \to \infty) = 0 \tag{20}$$

where C_{in} is the input concentration (the concentration behind the front). Equation (19) with boundary condtions (20) has the solution (Lichtner, 1988)

$$C(x') = \begin{cases} C_{\mathrm{in}}, & x' \leq 0 \\ C_{\mathrm{in}}\exp(a_1 x'), & x' > 0 \end{cases} \tag{21}$$

where

$$a_1 = \frac{1}{2}\Big(P - \sqrt{P^2 + 4\,E}\Big), \quad P = \frac{u'_D}{\phi_1 D} \tag{22}$$

and

$$E = \frac{K_d}{\phi_1 D}. \tag{23}$$

Zhao et al. (2008) derive an alternative solution for the concentration change around the front, which is different from equation (21) in two ways. Firstly, they assume that $c = c_{\rm eq}$ ($C = 0$) ahead of the front, and behind the front they apply a stationary solution of the convection-diffusion equation. We assume that $c = 0$ ($C_{\rm in} = C = -1$) behind the front and that the concentration is a solution of the stationary convection-diffusion and reaction equation ahead of the front. Secondly and most importantly, Zhao et al. (2008) ignore reaction in the stationary solution, which is different from the non-zero reaction rate in equation (21). The fact that solution (21) takes into account reaction can be used to make a condition for when 90% of the concentration change occupies a width $\Delta x'$. The concentration increases from $C = C_{\rm in}$ at the position of the front to $C_{\rm in}/10$ over the distance $\Delta x'$ a head of the front. The inequality $C(\Delta x') < 0.1\, C_{\rm in}$ gives that

$$K_d > \frac{1}{2}M'\Big(u'_D + \frac{1}{2}M'\phi\, D\Big) \tag{24}$$

where

$$M' = -\frac{2\ln(1/10)}{\Delta x'}. \tag{25}$$

Condition (24) gives a minimum dissolution rate for the concentration to change by 90% over a narrow zone that is less than $\Delta x'$. If the dissolution experiment is done in a box with length l_0 it is straightforward to rewrite the condition in terms of the Pe- and Da-numbers since we have assumed that $\phi = \phi_1$ ahead of the front and that we normally have $u'_D \approx u_D$. We then get the condition

$$\mathrm{Da} > \mathrm{Da}_{\rm min} = \frac{1}{2}M\left(\mathrm{Pe} + \frac{1}{2}M\right) \tag{26}$$

where M is the dimensionless version of M' given as $M = l_0 M'$. We can make an estimate of the M-number by choosing $\Delta x' = 0.02 l_0$, which gives that $M \approx 230$. Using a low value such as $\mathrm{Pe} = 10$ implies that $\mathrm{Da}_{\rm min} \approx 1.4 \cdot 10^4$ is a lower limit for Da-numbers that can give a front. Although the conditions (24) and (26) are based on a constant specific surface area function ($\hat{S} = 1$) they may serve as a valuable approximation for the general case of a $\hat{S}$-function.

It is so far assumed that the porosity makes a jump from ϕ_1 to ϕ_2 at the front position $x' = 0$. Approximation (21) for the concentration can be used to make an estimate for the porosity near the front. The concentration (21) is inserted into the porosity-equation (4), followed by a change in the integration variable from t to x', and then integrated. The integration is carried out

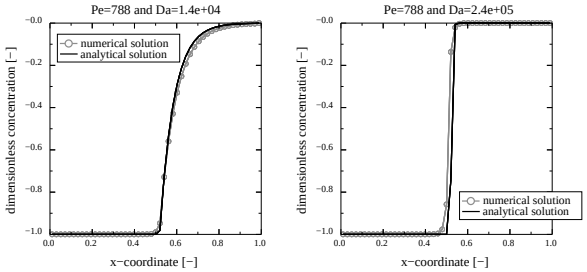

FIG. 2: The numerical and the approximate solutions for the concentration around the front.

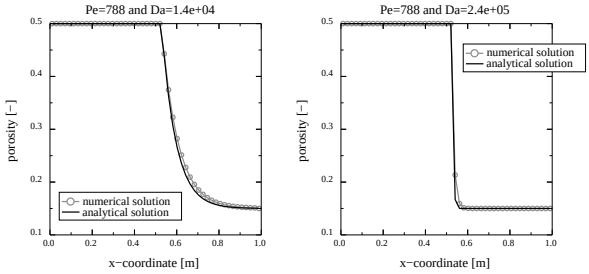

FIG. 3: The numerical and the approximate solutions for the porosity around the front.

with a specific surface area function that is $\hat{S}(\phi) = 1$ for $\phi < \phi_2$ and $\hat{S}(\phi) = 0$ for $\phi \geq \phi_2$. We then get that

$$\phi(x') = \begin{cases} \phi_2, & x' \leq 0 \\ \phi_1 + (\phi_2 - \phi_1)\exp(a_2 x'), & x' > 0 \end{cases} \tag{27}$$

The approximation is obtained by replacing the coefficient $\Delta\phi = -NK_d/a_1 v_f$ with $\Delta\phi = \phi_2 - \phi_1$. This replacement is a simple mean to assure that the approximation behaves correctly in the limit $x' \to \infty$. Alternatively, one could use the coefficient $\Delta\phi = -NK_d/a_1 v_f$ for ϕ in the porosity interval ϕ_1 to ϕ_2. Anyway, it is assumed that $-NK_d/a_1 v_f > \phi_2 - \phi_1$.

The numerical solution is compared against the concentration solution (21) in figure 2 and the match is quite good. This case has $\hat{S}(\phi) = 1$. The concentration plotted in figure 2b has 20 times faster dissolution rate than in figure 2a, as seen from the Da-numbers on the plots. The Da-numbers can be inserted into the condition (26) for having a narrow jump in the concentration. The Péclet-number $\mathrm{Pe} = 800$ and $M = 230$ gives that $\mathrm{Da}_{\rm min} = 1.05 \cdot 10^5$, which is in good agreement with the two plots in figure 2.

Figure 3 compares the numerical porosity against the porosity solution (27), which corresponds to the concentration profiles in figure 2. The porosity (27) is quite ac-

curate although it is based on a concentration solution that assumes a sharp step in the porosity at the front.

6. A STABILITY CRITERION FOR 3D REACTION FRONTS

The stability of a reaction front in a homogeneous 3D porous medium can be treated analytically by approximating a narrow reaction zone by a sharp front. Zhao et al. (2008) show that the velocity v_f of a sharp front is proportional to the Darcy flux u_D

$$\frac{v_f}{u_D} = N_f \tag{28}$$

where

$$N_f = \frac{M_f}{1+\phi_1 M_f}, \quad \text{and} \quad M_f = \frac{\mathcal{V}_s c_{\text{eq}}}{1-\phi_1}. \tag{29}$$

The normal case $\mathcal{V}_s c_{\text{eq}} \ll 1$ gives that $v_f/u_D \approx \mathcal{V}_s c_{\text{eq}}/(1-\phi_1)$.

The sharp front assumption implies that the porosity, permeability and the concentration are step functions at the front. The stability criterion is therefore for the limit of an infinitely rapid reaction. The assumption of a step-function in the concentration implies that transport of solute is by Darcy flow and not by diffusion, since the gradient of the concentration is zero everywhere, except at the front. The sharp front assumption is an approximation that covers the cases given as $\text{Pe} \gg 1$ and $\text{Da} \gg \text{Da}_{\min}$. The first condition ($\text{Pe} \gg 1$) says that convection dominates diffusion and the second condition ($\text{Da} \gg \text{Da}_{\min}$) assures that the front width is narrow.

The stability becomes expressed by a factor $\exp(\theta t)$ in the solution of the linearized equations for front position, pressure and Darcy flux, which implies that the front is unstable when $\theta > 0$. (See the Appendix for details.) The parameter θ is

$$\theta = N_f u_{D0} \sqrt{\left(\frac{2\pi}{\lambda_y}\right)^2 + \left(\frac{2\pi}{\lambda_z}\right)^2}\left(\frac{k_2-k_1}{k_2+k_1}\right) \tag{30}$$

where λ_y and λ_z are the wave lengths of the perturbations in y- and z-directions, respectively. The initial permeability ahead of the front is denoted by k_1 and the final permeability behind the front by k_2. The linear stability analysis gives that perturbations of a flat front with any wave-length are unstable as long as the permeability increases behind the front ($k_2 > k_1$). Similarly, perturbations of a flat front with any wave-length die out if the permeability decreases behind the front ($k_2 < k_1$). Finally, a perturbation remains unchanged if the reaction does not alter the permeability ($k_2 = k_1$).

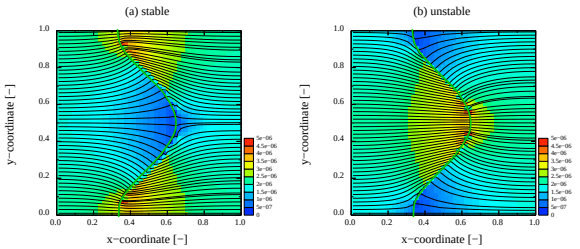

FIG. 4: (a) The permeability has decreased behind the front and the streamlines are focused towards the rear parts of the front. The Darcy flux is highest in the rear parts, these parts will catch up with the tip and the perturbation dies out. (b) The permeability has increased behind the front and the streamlines focuses towards the tip of the front. The Darcy flux is highest at the tip, the tip moves away from the other parts of the front and the front is unstable.

$$\begin{array}{ll} k_2 > k_1 & \text{unstable front: perturbations grow} \\ k_2 = k_1 & \text{labile front: perturbations are preserved} \\ k_2 < k_1 & \text{stable front: perturbations decrease} \end{array} \tag{31}$$

The linear stability analysis is carried out for homogeneous permeability fields at the two sides of the front, and it assumes that the reaction front moves with a velocity that is proportional to the Darcy flux. The stability condition (31) is considerably simpler than the stability criterion for reaction fronts in 2D porous media obtained by Chadam et al. (1987, 1988); Ortoleva et al. (1987); Xin et al. (1993) and more recently by Zhao et al. (2008). These authors also assume step functions in the porosity and the permeability across a sharp front, except for the concentration. They assume that the solute is in equilibrium downstream from the front, and they solve a convection-diffusion equation that ignores reaction for the upstream region. Furthermore, they assume that the normal derivative of the concentration at the front gives the front velocity.

The stability of a front perturbation depends on how it alters the fluid flow as shown by the simulations in figure 4. Notice that the flow is to the right and we recall that the velocity of a sharp front is proportional to the

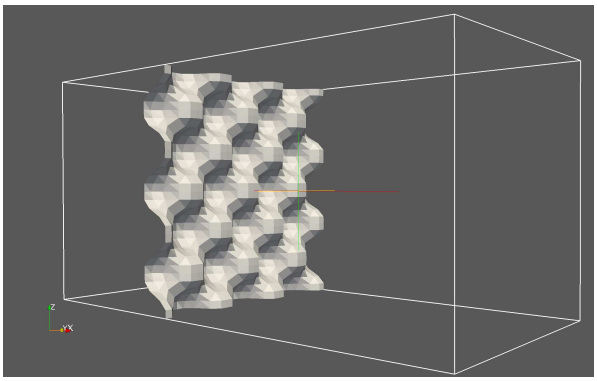

FIG. 5: The initial front perturbation.

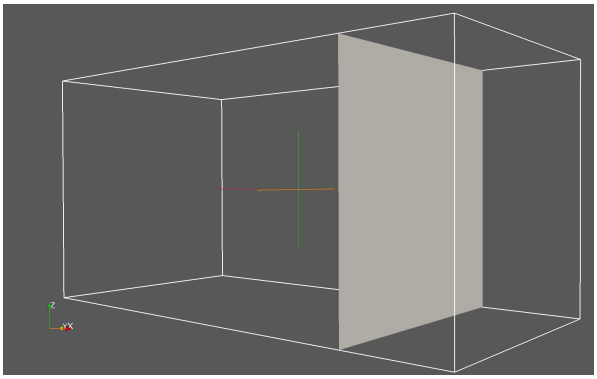

FIG. 6: The front in the stable case after the box has been flushed with 84.5 pore volumes.

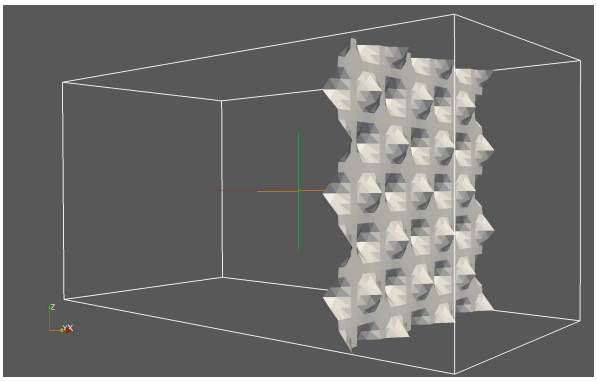

FIG. 7: The front in the labile case after the box has been flushed with 84.5 pore volumes.

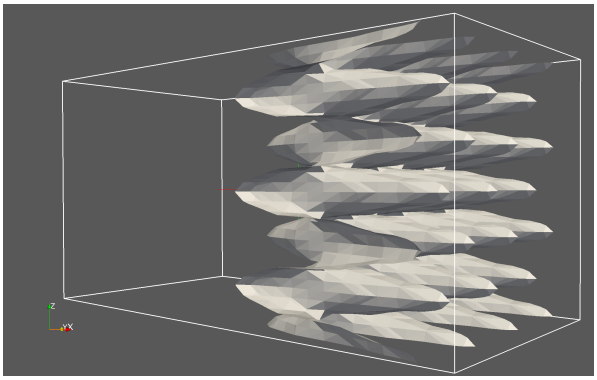

FIG. 8: The front in the unstable case after the box has been flushed with 84.5 pore volumes.

Darcy flux, as given by the ratio (28). Figure 4a shows that the stable case, with reduced permeability behind the front, has the fluid flow directed away from the head of the perturbation towards its rear parts. The Darcy flux and the front velocity are largest at the rear part of the front, which therefore will catch up with the head of the front, and the front becomes stable. Figure 4b shows the unstable situation when the permeability is larger behind the front. The Darcy flux and the front velocity are then largest at the tip of the perturbation, which then will "run" away from the rear parts. Chadam et al. (1988) have the same explanation for the instability. They show a sketch of how a perturbation focuses the flow field towards the head of the front, which is similar to the simulation shown in figure 4b.

The stability of reaction zones have been tested with a numerical solution of the three coupled equations (1), (3) and (4). The experiments are for a 3D box when $\mathrm{Pe} = 788 \gg 1$ and $\mathrm{Da} = 2.4{\cdot}10^5 > \mathrm{Da}_{\min}$. The other parameters are $c_{\mathrm{eq}}\mathcal{V}_s = 0.0075$ and $\phi_1 = 0.15$, which gives that $N_f = 0.0088$. The 3D grid has $30{\times}30{\times}30 = 27000$ cells and 63 time steps where used in each simulation. The linear equation system for the pressure equation is solved with a conjugate gradient solver with a Jacobi preconditioner, and the linear equation system for the concentration equation is solved with a GMRES-solver with a SOR preconditioner. An initial flat front that is normal to the x-axis is perturbed by $\Delta x = A\sin(2\pi y/\lambda{+}\theta_0)\sin(2\pi z/\lambda)$ where the offset is $\theta_0 = 3\pi/2$. Figure 5 shows the initial front where there are three wave lengths λ across the box in the y- and z-directions. The permeability is decreasing by an order of magnitude behind the front in the stable case, and figure 6 shows that the initial perturbation dies out and the front becomes flat. The decrease in permeability in rocks is normally the result of porosity decreasing from precipitation of minerals in the reaction zone. Figure 7 shows the labile case, where the permeability is unchanged behind the front and the initial perturbation moves forward almost unchanged. Finally, the unstable case is shown in figure 8, where an initial permeability is

increasing by an order of magnitude behind the front. The perturbation is then leading to unstable growth. The numerical examples indicate that the stability criterion applies to wide range of narrow reaction zones in porous media.

7. CONCLUSION

Two topics – (1) the width of reaction fronts and (2) the stability of reaction fronts in a 3D porous medium are studied with analytical and numerical modelling.

(1) We have derived approximate solutions for the stationary concentration- and porosity-profiles for the front. These stationary solutions have been used to derive a condition for a sharp front. The condition gives a minimum reaction rate necessary for 90% of the concentration change to take place inside a narrow band of a maximum width. The same condition has also been expressed in terms of the Péclet- and the Damköhler-number, when these numbers are based on the length of the system. Given an injection rate and the corresponding Péclet-number, the condition gives a minimum Damköhler-number necessary for 90% of the front to be restricted to 2% of the system length. The approximations for concentration and porosity through the reaction zone and the condition for a narrow reaction zone have been tested with numerical simulations.

(2) The stability of sharp reaction fronts is studied for a 3D porous media. It is shown, using linear stability analysis, that a perturbation of a flat and sharp front is unstable for all wave-lengths when the permeability increases behind the front. The sharp front is stable for perturbations if the permeability decreases behind the front. Finally, the perturbation remains unchanged if the permeability remains unchanged. For unstable fronts we show that perturbations with short wave lengths grow faster than perturbations with long wave lengths. The opposite applies for stable fronts – short wavelengths die out faster than long wave lengths. The stability of the reaction zones are also demonstrated with a numerical one-component reaction-convection-diffusion model. The stability criterion may be useful in the interpretation of the stability of reaction fronts in a wide variety of transport-reaction phenomena in porous media, although it is based on an approximation of the reaction zone as a sharp front.

ACKNOWLEDGEMENTS

This work has been partially funded by the SIS-project at IFE and partly by the SUCCESS center for CO2 storage under grant 193825/S60 from Research Council of Norway (RCN). SUCCESS is a consortium with partners from industry and science, hosted by Christian Michelsen Research as.

REFERENCES

Chadam, J., Hoff, D., Merino, E., Ortoleva, P., and Sen, A., Reactive infiltration instabilities, *IMA Journal of Applied Mathematics*, vol. **36**, pp. 207–220, 1987.

Chadam, J., Ortoleva, P., and Sen, A., A weakly nonlinear stability analysis of the reactive infiltration interface, *SIAM Journal on Applied Mathematics*, vol. **48**, pp. 1362–1378, 1988.

Cherry, J., Gilham, R., and Barker, J., 1984. Contaminants in groundwater: Chemical processes. National Academy Press, Washington, D.C, Ch. 3, pp. 46–64.

Daines, M. and Kohlstedt, D., The transition from porous to channelized flow due to melt/rock reaction during melt migration, *Geophysical Research Letters*, vol. **21**, no. 2, pp. 145–148, 1994.

Dewers, T. and Ortoleva, P., 1994. Formation of stylolites, marl/limestone alternations, and dissolution (clay) seams by unstable chemical compaction of argillaceous carbonates. Elsevier, New York, pp. 155–216.

Elsner, A., Wagner, A., Aste, T., Hermann, H., and Stoyan, D., Specific surface area and volume fraction of the cherry-pit model with packed pits, *Journal of Physical Chemistry B*, vol. **112**, pp. 7780–7784, 2009.

Hinch, E. and Bhatt, B., Stability of a acid front moving through porous medium, *Journal of Fluid Mechanics*, vol. **212**, pp. 279–288, 1990.

Lichtner, P., The quasi-stationary state approximation to coupled mass transport and fluid-rock interaction in a porous medium, *Geochimica et Cosmochimica Acta*, vol. **52**, no. 1, pp. 143–165, 1988.

Lichtner, P., Continuum Formulation of Multicomponent-Multiphase Reactive Transport, in Reactive Transport in Porous Media, eds. P. C. Lichtner, C. I. Steefel and E. H. Oelkers, *Reviews in Mineralogy*, vol. **34**, pp. 1–81, 1996.

Marle, C., *Multiphase flow in porous media*, Editions Technip (Paris), 1981.

Ortoleva, P., Chadam, J., Merino, E., and Sen, A., Geochemical self-organization II; the reactive-infiltration instability, *American Journal of Science*, vol. **287**, pp. 1008–1040, 1987.

Rege, S. and Fogler, H., Competition among flow, dissolution, and precipitation in porous media, *AIChE Journal*, vol. **35**, pp. 1177–1185, 1989.

Saffman, P. and Taylor, G., The penetration of a fluid into a medium of Hele-Shaw cell containing a more viscous liquid, *The Proceedings of the Royal Society of London, A*, vol. **58**, pp. 245–312, 1958.

Sherwood, J., Stability of a plane reaction front in a porous medium, *Chemical Engineering Science*, vol. **42**, no. 7, pp. 1823–1829, 1987.

Steefel, C. and Lasaga, A., 1990. The evolution of dissolution patterns: Permeability change due to coupled flow and reactions. American Chemical Society, Washington, pp. 212–225.

Szymczak, P. and Ladd, A., Wormhole formation in dissolving fractures, *Journal of Geophysical Research*, vol. **114**, no. B06203, pp. 1–22, 2009.

Szymczak, P. and Ladd, A., The initial stages of cave formation: Beyond the one-dimensional paradigm, *Earth and Planetary Science Letters*, vol. **301**, pp. 424–432, 2011.

Torquato, S., Random heterogeneous media: Microstructure and improved bounds on effective properties, *Applied Mechanics Reviews*, vol. **44**, no. 2, pp. 37–76, 1991.

Weissberg, H., Effective diffusion coefficent in porous media, *Journal of Applied Physics*, vol. **34**, no. 9, pp. 2636–2639, 1963.

Xin, J., Peirce, A., Chadam, J., and Ortoleva, P., Reactive flows in layered porous-media II. the shape stability of the reaction interface, *SIAM Journal on Applied Mathematics*, vol. **53**, no. 2, pp. 319–339, 1993.

Zhao, C., Hobbs, B., Hornby, P., Ord, A., Peng, S., and Liu, L., Theoretical and numerical analyses of chemical-dissolution front instability in fluid-saturated porous rocks, *International Journal for Numerical and Analytical Methods in Geomechanics*, vol. **32**, pp. 1107–1130, 2008.

APPENDIX A. THE STABILITY OF REACTION FRONTS IN 3D POROUS MEDIA

The analysis follows the presentation given by Marle (1981) for the linear stability analysis of an interface between two immiscible fluids in a Hele-Shaw cell. The stability analysis looks at how a small perturbation of a flat sharp front develops. The flat front is moving with a velocity v_{f0} along the x-axis, where the front velocity is related to the initial Darcy flux as $v_{f0} = N_f\, u_{D0}$. The initial Darcy flux u_{D0} gives that the pressure gradient at both side of the front is initially

$$\frac{dp_{i0}}{dx} = -\frac{\mu\, u_{D0}}{k_i} \tag{A.1}$$

where $i = 1, 2$. The index $i = 1$ denotes the unreacted part ahead of the front, and $i = 2$ is the reacted part behind the front. The pressure gradients (A.1) give that the initial fluid pressure is

$$p_{i0} = -\frac{\mu\, u_{D0}}{k_i}\Big(x - v_{f0}t\Big) \tag{A.2}$$

A reference value for the fluid pressure is arbitrary, and it is conveniently set to zero at position $x = 0$ at time $t = 0$. We will seek a solution for the deviation from the initial state when the linear front is subjected to a small perturbation $h(y, z, t)$. The fluid pressure and the Darcy flux can then be written as

$$p_i = p_{i0} + p_i' \qquad \text{and} \qquad \mathbf{v}_i = (u_{D0}, 0, 0) + \mathbf{v}_i' \qquad i = 1, 2 \tag{A.3}$$

where the initial Darcy flux is

$$(u_{D0}, 0, 0) = \mathbf{v}_0 = -\frac{k_i}{\mu}\nabla p_{i0} \tag{A.4}$$

and where the primed quantities p_i' and $\mathbf{v}_i'$ are the deviations caused by the perturbation of the front. The equation for the deviation in Darcy flux becomes

$$\mathbf{v}_i' = \mathbf{v}_i - \mathbf{v}_0 = -\frac{k_i}{\mu}\nabla p_i' \quad \text{for} \quad i = 1, 2 \tag{A.5}$$

and from fluid conservation we get the continuity equation for the deviations in the fluid velocity

$$\nabla \cdot \mathbf{v}_i' = \nabla \cdot (\mathbf{v}_i - \mathbf{v}_0) = 0 \quad \text{for} \quad i = 1, 2. \tag{A.6}$$

Conservation of fluid through the front, $\mathbf{v}_1 \cdot \mathbf{n} = \mathbf{v}_2 \cdot \mathbf{n}$, gives that

$$\mathbf{v}_1' \cdot \mathbf{n} = \mathbf{v}_2' \cdot \mathbf{n} \tag{A.7}$$

and continuity of the pressure at the front, $p_1 = p_2$, gives that

$$p_2'-p_1' = -(p_{20}-p_{10}) = \left(\frac{1}{k_2} - \frac{1}{k_1}\right)\mu\, u_{D0}\left(x-v_{f0}t\right). \tag{A.8}$$

The next step is a change of x-coordinate to $x' = x-v_{f0}t$, which is a coordinate system that follows the initially flat front. The position of the perturbed front in the x'-coordinate system is simply $x' = h(y,z,t)$, and the velocity of the perturbed front in x'-coordinate system is

$$v_f - v_{f0} = \frac{\partial h}{\partial t}. \tag{A.9}$$

The unit normal vector of the front $x' = h(y,z,t)$ is

$$\mathbf{n} = \frac{(1, -\partial h/\partial y, -\partial h/\partial z)}{\left(1+(\partial h/\partial y)^2 + (\partial h/\partial z)^2\right)^{1/2}} \tag{A.10}$$

and

$$\mathbf{n} \approx (1, -\frac{\partial h}{\partial y}, -\frac{\partial h}{\partial z}) \tag{A.11}$$

when it is approximated to first order in $\partial h/\partial y$ and $\partial h/\partial z$. The deviations $\mathbf{v}_i' = (u_i', v_i', w_i')$, p_i' and h and their derivatives are infinitesimal quantities, and we have to first order in these quantities that

$$\mathbf{v}_i' \cdot \mathbf{n} \approx u_i' - \frac{\partial h}{\partial y}v_i' - \frac{\partial h}{\partial z}w_i' \approx u_i'. \tag{A.12}$$

The equation for the front velocity is

$$\frac{\partial h}{\partial t} = v_f - v_{f0} = N_f\,(u_D - u_{D0}) = N_f\, u_i' \tag{A.13}$$

The first order equations for the infinitesimal deviations are summarized as follows

$$u_i' = -\frac{k_i}{\mu}\frac{\partial p_i'}{\partial x'}, \quad v_i' = -\frac{k_i}{\mu}\frac{\partial p_i'}{\partial y}, \quad w_i' = -\frac{k_i}{\mu}\frac{\partial p_i'}{\partial z}, \tag{A.14}$$

and

$$\frac{\partial u_i'}{\partial x} + \frac{\partial v_i'}{\partial y'} + \frac{\partial w_i'}{\partial z'} = 0 \tag{A.15}$$

in each subdomain ($i = 1, 2$), and as

$$p_2'-p_1' = (\frac{1}{k_2}-\frac{1}{k_1})\mu\, u_{D0}\, h \text{ and } \frac{\partial h}{\partial t} = N_f\, u_1' = N_f\, u_2' \tag{A.16}$$

at the front $x' = x - v_{f0}t = h$. The equations (A.14), (A.15) and (A.16) are supplied by the boundary conditions

$$u_1' = v_1' = w_1' = p_1' = 0 \quad \text{for} \quad x' \to \infty \tag{A.17}$$

and

$$u_2' = v_2' = w_2' = p_2' = 0 \quad \text{for} \quad x' \to -\infty \tag{A.18}$$

which says that the deviations are zero at an infinite distance away from the front. Following Marle (1981), the linear equations (A.14), (A.15) and (A.16) with boundary conditions (A.17) and (A.18) have a solution of the following form

$$h(y,t) = A\exp\left(\frac{2\pi j y}{\lambda_y} + \frac{2\pi j z}{\lambda_z} + \theta t\right) \tag{A.19}$$

$$u_i'(x',y,z,t) = B_i\exp\left(\frac{2\pi j y}{\lambda_y} + \frac{2\pi j z}{\lambda_z} + \sigma_i x' + \theta t\right) \tag{A.20}$$

$$v_i'(x',y,z,t) = C_i\exp\left(\frac{2\pi j y}{\lambda_y} + \frac{2\pi j z}{\lambda_z} + \sigma_i x' + \theta t\right) \tag{A.21}$$

$$w_i'(x',y,z,t) = D_i\exp\left(\frac{2\pi j y}{\lambda_y} + \frac{2\pi j z}{\lambda_z} + \sigma_i x' + \theta t\right) \tag{A.22}$$

$$p_i'(x',y,z,t) = E_i\exp\left(\frac{2\pi j y}{\lambda_y} + \frac{2\pi j z}{\lambda_z} + \sigma_i x' + \theta t\right) \tag{A.23}$$

where $i = 1, 2$ and the $j = \sqrt{-1}$. The solution is for a perturbation with a wave-length λ_y in the y-direction and a wave-length λ_z in the z-direction. When these expressions are inserted into equations (A.14) and (A.15) for the subdomains, we get that

$$B_i = -\frac{k_i}{\mu}\sigma_i E_i, \quad C_i = -\frac{k_i}{\mu}\frac{2\pi j}{\lambda_y}E_i, \quad D_i = -\frac{k_i}{\mu}\frac{2\pi j}{\lambda_z}E_i, \tag{A.24}$$

and

$$\sigma_i B_i + \frac{2\pi j}{\lambda_y}C_i + \frac{2\pi j}{\lambda_z}D_i = 0 \tag{A.25}$$

and when inserted into the conditions (A.16) at the front, we have that

$$N_f B_1 = N_f B_2 = A\theta, \text{ and } E_2-E_1 = (\frac{1}{k_2}-\frac{1}{k_1})\mu\, u_{D0} A \tag{A.26}$$

From equations (A.24) and (A.25) we get that

$$\sigma_i^2 = \left(\frac{2\pi}{\lambda_y}\right)^2 + \left(\frac{2\pi}{\lambda_z}\right)^2 \tag{A.27}$$

and the boundary conditions (A.17) and (A.18) imply that

$$\sigma_1 = -\sigma_0, \quad \sigma_2 = \sigma_0 \text{ where } \sigma_0 = \sqrt{\left(\frac{2\pi}{\lambda_y}\right)^2 + \left(\frac{2\pi}{\lambda_z}\right)^2} \tag{A.28}$$

Expressions (A.24) and (A.25) now give that

$$E_i = -\frac{\mu B_i}{k_i \sigma_i} \tag{A.29}$$

and therefore

$$E_1 = \frac{\mu\theta A}{k_1 N_f \sigma_0} \quad \text{and} \quad E_2 = -\frac{\mu\theta A}{k_2 N_f \sigma_0} \tag{A.30}$$

When E_1 and E_2 are inserted into the second equality (A.26) we have finally that

$$-\Big(\frac{1}{k_2} + \frac{1}{k_1}\Big)\frac{\theta}{N_f \sigma_0} = \Big(\frac{1}{k_2} - \frac{1}{k_1}\Big) u_{D0} \tag{A.31}$$

which gives equation (30) for θ.

Captions

Figure 1: Black is solid and white is void space. (a) Pore space between grains. (b) Pore space as holes in well cemented rock.

Figure 2: The numerical and the approximate solutions for the concentration around the front.

Figure 3: The numerical and the approximate solutions for the porosity around the front.

Figure 4: (a) The permeability has decreased behind the front and the streamlines are focused towards the rear parts of the front. The Darcy flux is highest in the rear parts, these parts will catch up with the tip and the perturbation dies out. (b) The permeability has increased behind the front and the streamlines focuses towards the tip of the front. The Darcy flux is highest at the tip, the tip moves away from the other parts of the front and the front is unstable.

Figure 5: The initial front perturbation.

Figure 6: The front in the stable case after the box has been flushed with 84.5 pore volumes.

Figure 7: The front in the labile case after the box has been flushed with 84.5 pore volumes.

Figure 8: The front in the unstable case after the box has been flushed with 84.5 pore volumes.